A computational framework to unify representation similarity and function in biological and artificial neural networks

Xuming Ran[1], **Jie Zhang**[2,3], **Ziyuan Ye**[1], **Haiyan Wu**[4], **Qi Xu**[5],
Huihui Zhou[6,*], **Quanying Liu**[1,*]

[1]Southern University of Science and Technology, China
[2]Shenzhen Institutes of Advanced Technology, Chinese Academy of Sciences, China
[3]University of the Chinese Academy of Sciences, China
[4]Centre for Cognitive and Brain Sciences and Department of Psychology, University of Macau
[5]School of Artificial Intelligence, Dalian University of Technology, China
[6]Pengcheng Laboratory, China

Abstract

Artificial neural networks (ANNs) are powerful tools for studying neural representations in the ventral visual stream of the brain, which, in turn, have inspired new designs of ANN models to improve task performance. However, a unified framework for merging these two directions has been lacking so far. In this study, we propose an integrated framework called Deep Autoencoder with Neural Response (DAE-NR), which incorporates information from the visual cortex into ANN models to achieve better image reconstruction performance and higher neural representation similarity between biological and artificial neurons. The same visual stimuli (*i.e.*, natural images) are input to both the mice brain and DAE-NR. The encoder of DAE-NR jointly learns the dependencies from neural spike encoding and image reconstruction. For the neural spike encoding task, the features derived from a specific hidden layer of the encoder are transformed by a mapping function to predict the ground-truth neural response under the constraint of image reconstruction. Simultaneously, for the image reconstruction task, the latent representation obtained by the encoder is assigned to a decoder to restore the original image under the guidance of neural information. In DAE-NR, the learning process of encoder, mapping function and decoder are all implicitly constrained by these two tasks. Our experiments demonstrate that *if and only if* with the joint learning, DAE-NRs can improve the performance of visual image reconstruction and increase the representation similarity between biological neurons and artificial neurons. The DAE-NR offers a new perspective on the integration of computer vision and neuroscience.

1 Introduction

Computer vision has achieved almost comparable performance to the human visual system on some tasks, mainly thanks to recent advances in deep learning. Image reconstruction is one of the essential tasks in computer vision Wang et al. (2018); Ravishankar et al. (2020). As a solution, the auto-encoder (AE) framework embeds the high-dimensional input to a low-dimensional latent space by the encoder and then reconstructs the image by the decoder Hinton & Salakhutdinov (2006); Goodfellow et al. (2016). Inspired by neuroscience, computer vision researchers have been interested in how to use information from biological neurons to achieve brain-like performance (such as robustness and ability to learn from small samples). The biology-inspired AE models may help improve performance in image reconstruction tasks and bring biological interpretability Federer et al. (2020); Schrimpf et al. (2018); Safarani et al. (2021). To this end, the key question is how to integrate biological information into AEs.
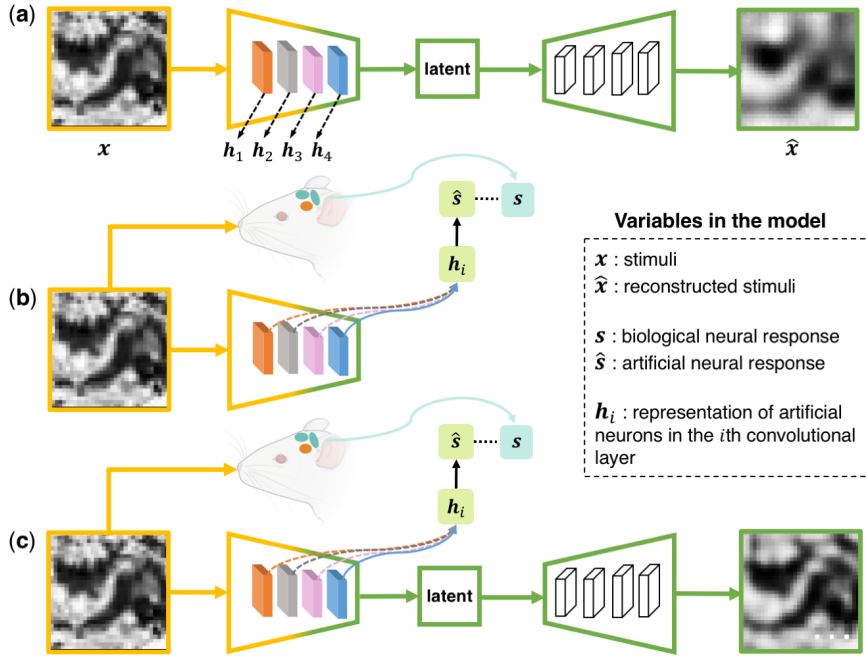
Figure 1: Scheme of the models: (a) the standard deep autoencoder (DAE) for image reconstruction, (b) the convolutional neural network with factorized readout (CNN-FR) for predicting neural responses, (c) the DAE with neuron response (DAE-NR) for both image reconstruction and neural response prediction. s denotes the biological neural response; $\hat{s}$ denotes the prediction of biological neural response; $\mathbf{h}_i$ ($i \in \{1, 2, 3, 4\}$) is the feature map of the ith convolutional layer.

On the other hand, computational neuroscience is interested in building models that map stimuli to neural responses. Traditional models have difficulty expressing nonlinear characteristics between stimulus and neural response. Deep learning empowers computational neuroscience models and reveals the relationship between stimuli and neural spikes Klindt et al. (2017) Although biological and artificial neural networks may have fundamental differences in computation and learning Macpherson et al. (2021), both are realized by interconnected neurons: the former by biological neurons; the latter by artificial neurons. Some previous work has focused on investigating the similarities between the information representation of biological neurons and artificial neurons using end-to-end ANNs, suggesting that artificial neurons in different layers of ANNs share similar representations with biological neurons in brain regions along the ventral visual pathway DiCarlo et al. (2012); Yamins & DiCarlo (2016); Walker et al. (2019); Bashivan et al. (2019). However, how to build artificial neural networks most similar to biological neural representations remain an open question.

Some studies have leveraged real neural responses to speed up the training process and improve network performance in object detection tasks Federer et al. (2020); Schrimpf et al. (2018); Safarani et al. (2021). However, no model has yet utilized neural responses as constraints to improve image reconstruction performance. More importantly, to our knowledge, there is no unified framework that can leverage both neural responses to improve model performance and image reconstruction tasks to improve representational similarity between biological and artificial neurons.

In this paper, we aim to tackle these two questions in one piece. Specifically, we propose a united biologically inspired framework, which jointly learns i) to project features of visual input in a specific layer of the encoder to biological neural responses by a mapping function and ii) to reconstruct the visual input via the decoder. As a result, its encoder has a higher representational similarity to the real neural responses, and its decoder achieves better image reconstruction performance. Our contributions can be summarized as follows.
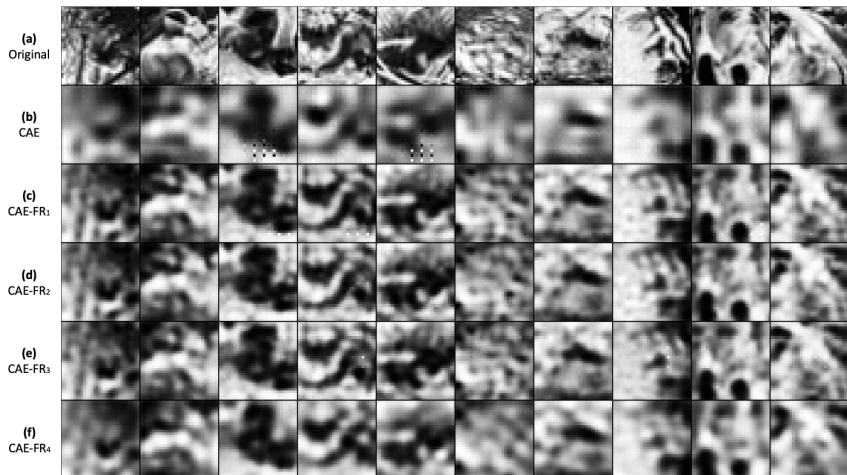
Figure 2: Reconstructed images of neural activity in mouse Region 3. From top to bottom, each row displays 10 examples of the original stimuli images (a), the reconstructed images by CAE (b), and by CAE-FR$_i$ (c-f) for $i \in \{1, 2, 3, 4\}$, respectively.

- We present a biologically inspired framework called Deep Autoencoder with Neural Response (DAE-NR). The framework can simultaneously learn to predict neural responses and to reconstruct the visual stimuli (**Sec.3**).

- The deep autoencoders embedded in DAE-NR can improve the image reconstruction quality with the help of a Poisson loss on the predicted neural activity, compared to the baseline auto-encoder models (**Sec.4.2 & 4.4**).

- The computational neuroscience model (CNM) via DAE-NR offers higher resemblance between artificial neurons and biological neurons compared to the competing end-to-end CNM models (**Sec.4.3 & 4.4**).

2 RELATED WORK

Image reconstruction via auto-encoders: A big breakthrough in image reconstruction is in Hinton & Salakhutdinov (2006), which equips an autoencoder with a stack of restricted Boltzmann machines. The denoising autoencoder Vincent et al. (2008) and convolutional autoencoder (CAE) Masci et al. (2011) further improve the stability of autoencoders by adding noise and taking advantage of convolutional layers in feature extraction, respectively. Variational Autoencoder (VAE) enhances model robustness of generating insightful representations through a latent distribution learning mechanism Kingma & Welling (2014). Vector quantisation VAE (VQ-VAE) employs the vector quantisation to obtain a discrete latent representation that can improve the quality of image reconstruction and generation van den Oord et al. (2017). Recent advances follow a similar trend of latent space exploration and generalize variants of DAE to many domains Larsen et al. (2016); Khattar et al. (2019); Park et al. (2020); Wang et al. (2021); Cai et al. (2021); Ran et al. (2021). However, However, DAE and its variants in image reconstruction suffer from the same problem; the parameters have a high degree of freedom. In other words, parameters can only be learned through error backpropagation guided by gradients. Therefore, some meaningful constraints on the parameter space will be beneficial for learning.

Neural similarity in computational neuroscience: Many models in computational neuroscience have been proposed to build a relationship between stimuli and the corresponding neural spike responses, which are known as neural spike encoding. The goal of these models is to increase the similarity between predicted and true neural responses. Historically, much effort has been devoted to finding tuning curves for specific features of visual stimuli, such as the orientation of bars, to predict neural responses (Carandini et al., 2005; Dräger, 1975; Hubel & Wiesel, 1962; 1968; Niell et al., 2008). This is feasible for some neurons in the primary visual cortex, but not for all neurons. Nonlinear methods provide a more general approach to predicting neural responses,

including energy models Hubel & Wiesel (1962), the linear-nonlinear (LN) model and the LN-LN model Meyer et al. (2017). Traditional machine learning methods, such as generalized linear models (GLMs) (Willmore et al., 2008), the multi-layer perceptron (MLP) and the support vector regression (SVR) Das et al. (2019), have been widely applied in computational neuroscience to predict the neural responses to stimuli. More recently, hierarchical structures have been found in both ventral visual pathway (DiCarlo et al., 2012; Vintch et al., 2015; Rowekamp & Sharpee, 2017) and in deep convolutional neural networks (Fukushima et al., 1983; LeCun et al., 1989; Krizhevsky et al., 2012). Underlying the similar hierarchy, the brain and CNN are believed to share similar neural representations for extracting features from stimuli layer by layer, from simple to complex. To test this hypothesis, Yamins el al.Yamins & DiCarlo (2016) proposed to use hierarchical CNNs as computational neuroscience models to investigate neural similarity. They report neural representation similarities between biological neurons along the ventral visual stream and artificial neurons in different convolutional layers Yamins & DiCarlo (2016). Furthermore, CNN with a fully-connected readout layer (CNN-FC) can directly map the convolutional features to neural responses McIntosh et al. (2016). However, such a fully-connected readout layer typically contains a large number of parameters. To reduce the number of parameters in the readout layer, CNN with a factorized readout layer (CNN-FR) and CNN with a fixed mask (CNN-FM) are proposed which factorize convolutional features into a spatial mask Klindt et al. (2017). So far, CNN models with readout layers have become an important tool for studying neural similarity between the brain and CNN.

3 METHOD

Here we first introduce the notation of data spaces and variables. We then present the framework of deep autoencoders with neural response (DAE-NR) in Sec. 3.1. Finally, we describe realizations of the DAE-NR framework using CAE and CNN-FR in Sec. 3.2.

The data space of visual stimuli, the neural responses, and the features of stimuli in the i-th convolutional layer are denoted by $\mathcal{X}$, $\mathcal{S}$, and $\mathcal{H}_i$. The visual stimuli (*i.e.*, natural images) and the corresponding neural responses (*i.e.*, neural spikes in the V1 region) are represented as $\boldsymbol{x} \in \mathbb{R}^{N \times P \times P \times C}$ and $\boldsymbol{s} \in \mathbb{R}^{N \times M}$, respectively. The features of stimuli in the i-th convolutional layer are denoted as $\boldsymbol{h}_i \in \mathbb{R}^{N \times K \times K \times F}$, with the sample size ($N$), the image resolution (P), the image channel (C), the kernel size of a feature of stimuli (K), the number of kernels (F), and the number of V1 neurons (M), respectively.

3.1 THE DAE-NR FRAMEWORK

The DAE-NR combines the function of DAE for image reconstruction and the role of CNM for predicting neural responses. The DAE-NR framework consists of three parts, including an encoder $f_1: \mathcal{X} \to \mathcal{H}_i$, a decoder $f_2: \mathcal{H}_i \to \hat{\mathcal{X}}$, and a mapping function $f_3: \mathcal{H}_i \to \hat{\mathcal{S}}$.

DAE: The standard DAEs and their variants (*e.g.*, CAE Masci et al. (2011), VAE (Kingma & Welling, 2014) and VQ-VAE (van den Oord et al., 2017)) consist of an encoder, the latent space, and a decoder, which have become mainstream models for image reconstruction. In our work, instead of separating the encoder and decoder by the latent layer, we split the encoder and decoder at the i-th layer of DAE. In this way, the architecture of our DAE turns to be: (i) an encoder $f_1: \mathcal{X} \to \mathcal{H}_i$, to embed the input to neural representation in i-th layer; (ii) a decoder $f_2: \mathcal{H}_i \to \hat{\mathcal{X}}$, to reconstruct the input based on neural representations in i-th layer. We formally describe them as follows:

$$\begin{aligned} \text{the encoder: } & \boldsymbol{h}_i = f_1(\phi_1, \boldsymbol{x}), \\ \text{the decoder: } & \hat{\boldsymbol{x}} = f_2(\phi_2, \boldsymbol{h}_i), \end{aligned} \tag{1}$$

where the $\hat{\boldsymbol{x}}$ is reconstructed from the original image $\boldsymbol{x}$. Both the encoder and decoder are realized by neural networks with parameters ϕ_1 and ϕ_2, respectively. The goal of DAE is to reconstruct the image by optimizing the the loss function $\mathcal{L}(\phi_1, \phi_2)$.

CNM: The computational neuroscience models (*e.g.*, CNN-FR (Klindt et al., 2017; Bashivan et al., 2019), CNN-FC (McIntosh et al., 2016), and CNN-FM (Klindt et al., 2017)) usually consist of the encoder and the readout layer. The encoder can be used to extract the image's features. The readout layer is used to map the feature space $\mathcal{H}_i$ to the neural responses in the space $\mathcal{S}$. The mapping

function $f_3 : \mathcal{H}_i \to \hat{\mathcal{S}}$ is

$$\hat{s} = f_3(h_i, \theta). \tag{2}$$

We employ the $\mathcal{L}(\theta)$ loss to optimize the representation similarity between artificial neurons (*i.e.*, $\hat{s}$) and biological neurons neurons (*i.e.*, s) in the mapping function.

The loss function of DAE-NR explicitly considers both the image reconstruction task in computer vision and the neural representation similarity task in computational neuroscience, as defined in Eq. equation 3.

$$\mathcal{L}(\phi_1, \phi_2, \theta) = \alpha * \mathcal{L}(\phi_1, \phi_2) + \beta * \mathcal{L}(\theta), \tag{3}$$

where α and β are the hyperparameters to trade off the image reconstruction task and the neural representation similarity task.

3.2 REALIZATIONS OF DAE-NR

Here, we first realize DAE-NR by a toy model (*i.e.*, CAE-FR) combining a convolutional autoencoder (CAE) and a CNN with factorized readout (CNN-FR). It is important to note that the DAE-NR framework is compatible with different instantiations. We have full implementation in Table 1.

CAE: Both the encoder and the decoder are realized by convolutional neural networks with parameters ϕ_1 and ϕ_2, respectively. The loss function of CAE is formulated as a L_2 norm:

$$\mathcal{L}(\phi_1, \phi_2) = \|x - \hat{x}\|_2^2 = \|x - f_2(\phi_2, f_1(\phi_1, x))\|_2^2, \tag{4}$$

where the $\hat{x}$ is reconstructed from the original image x.

CNN-FR: The CNN-FR consists of two parts, the convolutional layers as the encoder and the factorized readout layer (Klindt et al., 2017; Bashivan et al., 2019; Cadena et al., 2019; Zhuang et al., 2021). The convolutional layers convolve the image with a number of kernels followed by batch normalization, resulting in multiple feature maps. The readout layer pools the output of the convolutional layer (*i.e.*, h_i) by applying a sparse mask on each neuron. Let us denote that h_i lies in the feature space $\mathcal{H}_i$ and the neural responses in the space $\mathcal{S}$. The mapping function is

$$\hat{s} = f_3(h_i, \theta_{\mathrm{s}}, \theta_{\mathrm{d}}) = \left[\sum (\theta_{\mathrm{s}} \cdot h_i)\right] * \theta_{\mathrm{d}} + b, \tag{5}$$

where θ_{s} is the spatial mask, θ_{d} is the weights sum of all features h_i, and b is the bias. We use the Poisson loss to optimize the representation similarity between artificial neurons (i.e. $\hat{s}$) and biological neurons neurons (i.e. s) in the mapping function as Eq.(6),

$$\mathcal{L}(\theta_{\mathrm{s}}, \theta_{\mathrm{d}}) = \sum (\hat{s} - s \log \hat{s}). \tag{6}$$

Previous studies have shown that the responses of V1 neurons to natural stimuli are sparse, and the activity of neural populations with higher sparseness exhibits greater discrimination against natural stimuli. (Vinje & Gallant, 2000; Weliky et al., 2003; Froudarakis et al., 2014; Yoshida & Ohki, 2020). Likewise, (Zhuang et al., 2017) has reported that the resemblance between the representation of biological neurons and artificial neurons in higher convolutional layers exists only under the sparsity constraint on the CNN, regardless of any other factors (*e.g.*, , model structure, training algorithm, receptive field size, and property of training stimuli). In our study, the representational similarity of V1 neurons is brought to a specific layer of the CAE encoder ($h_i, i \in [1, 2, 3, 4]$) with the sparsity constraint for artificial neurons in this layer.

CAE-FR: The CAE-FR combines the function of CAE and CNN-FR. The loss of CAE-FR explicitly considers both the image reconstruction task and the neural representation similarity task, as defined in Eq. equation 7,

$$\mathcal{L}(\phi_1, \phi_2, \theta_{\mathrm{s}}, \theta_{\mathrm{d}}) = \alpha * \|x - f_2(\phi_2, f_1(\phi_1, x))\|_2^2 + \beta * \sum (f_3(h_i, \theta_{\mathrm{s}}, \theta_{\mathrm{d}}) - s \log f_3(h_i, \theta_{\mathrm{s}}, \theta_{\mathrm{d}})). \tag{7}$$

Intuitively, the larger α favors the reconstruction task, while the larger β biases toward the neural representation similarity task.

Table 1: The variants of DAE-NR. The implementation details of CAE-FR are presented in Sec 3.2. The implementation of other variants is the same as CAE-FR.

DAEs CNMs	CAE	VAE	VQ-VAE
CNN with factorized readout (CNN-FR)	**CAE-FR**	VAE-FR	VQ-VAE-FR
CNN with fully-connected readout (CNN-FC)	CAE-FC	VAE-FC	VQ-VAE-FC
CNN with fixed mask (CNN-FM)	CAE-FM	VAE-FM	VQ-VAE-FM

4 EXPERIMENTS AND RESULTS

4.1 EXPERIMENTAL SETTINGS

Datasets: We conduct experiments on a publicly available dataset with the gray-color images as visual stimuli and the corresponding neural responses. The neural response dataset is obtained from Antolík et al. (2016). The neural responses in the dataset are recorded in three regions in the primary visual cortex (V1) of sedated mice visually stimulated with the natural images (See Appendix Fig. 5). The number of neurons over the three brain regions is shown in the Appendix Table 7.

Models: We realized DAE-NRs with nine different combinations of DAE and CNM (See Table 1). DAE-NRs are compared with DAE baselines for the image reconstructions task and compared with CNM baselines for the neural representation similarity task. We choose CAE, VAE and VQ-VAE as the DAE baselines and CNN-FR, CNN-FC and CNN-FM as the CNM baselines, respectively. Especially, we have the CNM with $\mathbf{h}_i$ (CNM$_i$, $i \in \{1, 2, 3, 4\}$). The CNM in DAE-NR can be readout from four different convolutional layers (*i.e.*, $\mathbf{h}_i$ of the DAE encoder), resulting in four variants of DAE-NRs (*i.e.*, DAE-NR$_i$, $i \in \{1, 2, 3, 4\}$) which represent the CNM extracted from the different convolutional layers $\mathbf{h}_i$.

Network architectures: The architecture of the DAE in DAE-NR is 48C23-48C13-48C23-48C13-48DC13-48DC23-48DC13-1DC23 (kCnm and kDCnm indicates k filters in the convolutional and deconvolutional layer, n stride and m filters). The dimension of latent variable in CAE and VAE is set as 100; the prior of VAE and VQ-VAE is the Gaussian distribution $N(0, 1)$ and uniform distribution, respectively. The dimension of latent embedding space in VQ-VAE is 32×256. Each convolutional layer is followed by a batch normalization with an ELU activation function, while the activation function in the final layer for image reconstruction is $tanh$. The CNM in DAE-NR shares the four different convolutional layers ($\mathbf{h}_1$, $\mathbf{h}_2$, $\mathbf{h}_3$, and $\mathbf{h}_4$). The CNM in DAE-NR can be readout from four different convolutional layers (i.e. $\mathbf{h}_i$ of the encoder of DAE), so there are four variants of DAE-NR, i.e. DAE-NR$_i$, $i \in \{1, 2, 3, 4\}$ representing the CNM extracted from the different convolutional layers $\mathbf{h}_i$.

Training procedures: We preprocess the images (i.e., reshape the size of the natural image to $32 \times 32 \times 1$ and normalize the intensity of the image to [-1,1]) and then input them to the model. The model is trained with an initial learning rate of 0.001, and the early stopping strategy is applied based on a separated validation set. If the error in the validation set does not improve by 1000 steps, we return the best parameter set, reduce the learning rate by two, and train in the second time.The VAE is optimized by the evidence lower bound ($ELBO$), while the VQ-VAE is optimized following the settings in (van den Oord et al., 2017). The settings of hyperparameters for tasks in Sec 4.2 and Sec 4.3 are detailed in Appendix Table 8 and 9 , respectively. The Appendix Table 10 and Table 11&12&13 are the settings the hyperparameters of different DAE-NR variants for image reconstruction on Region 3 and neural similarity experiments on Region 1,2 and 3 in Sec 4.4, respectively.

Tasks: There are two tasks in the experiment: 1) the image reconstruction (IR) task and 2) the neural representation similarity (NRS) task. We apply CAE-FR to analyse the effects of neural responses on IR and the effects of image reconstruction on NRS tasks in DAE-NR. We compare the other DAE-NR variants with DAE and CNM for IR and NRS tasks to explore the generalisation capability of DAE-NR. In the IR task, we use the mean squared error (MSE↓), structural similarity (SSIM↑) Wang et al. (2004), and peak signal-to-noise ratio (PSNR↑) Wang et al. (2004) as metrics to

Table 2: The quantitative results of image reconstruction with all neurons in the region 1, 2, and 3, respectively. The best result in each region under different metrics is highlighted with boldface.

Region	Region 1			Region 2			Region 3		
Metric / Model	MSE↓	PSNR↑	SSIM↑	MSE↓	PSNR↑	SSIM↑	MSE↓	PSNR↑	SSIM↑
CAE	0.022	23.709	0.771	0.024	23.338	0.754	0.081	17.039	0.561
CAE-FR$_1$	**0.021**	**23.829**	**0.776**	**0.023**	23.392	0.753	0.044	19.751	0.763
CAE-FR$_2$	**0.021**	23.779	0.775	**0.023**	23.440	0.759	**0.043**	**19.819**	**0.764**
CAE-FR$_3$	**0.021**	23.778	0.775	0.024	23.330	0.755	**0.043**	19.789	0.761
CAE-FR$_4$	0.022	23.721	0.773	**0.023**	**23.491**	**0.760**	0.059	18.462	0.668

Table 3: The quantitative results of image reconstruction with constraints of significant neurons and insignificant neurons in the region 3. The best result under different metrics is highlighted with boldface.

Metric	MSE↓		SSIM↑		PSNR↑	
Significant? / Model	✓	×	✓	×	✓	×
CAE-FR$_1$	**0.043**	0.125	**0.761**	0.332	**19.784**	15.168
CAE-FR$_2$	**0.047**	0.082	**0.743**	0.547	**19.467**	16.970
CAE-FR$_3$	**0.049**	0.116	**0.724**	0.362	**19.245**	15.463
CAE-FR$_4$	0.047	**0.045**	0.740	**0.752**	19.497	**19.628**

quantify the image reconstruction performance[1]. We compare the DAE-NR$_1$, DAE-NR$_2$, DAE-NR$_3$ and DAE-NR$_4$ with the standard DAE. In the NRS task, we use Pearson correlation coefficient (PCC↑) as a metric to quantitatively evaluate models. We implement the traditional end-to-end CNM$_i$ ($i \in \{1, 2, 3, 4\}$) as baseline models.
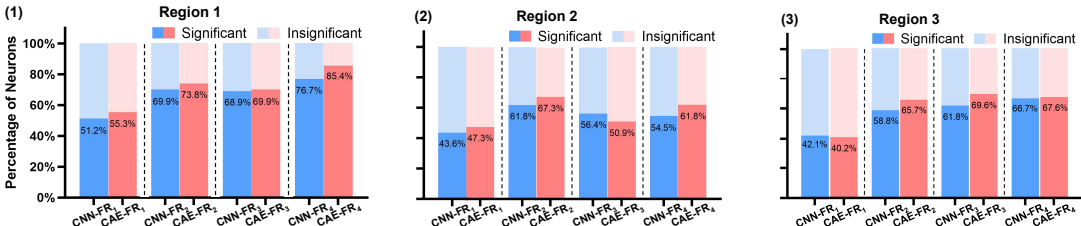
Figure 3: The number of significant neurons (deep blue and deep red) and insignificant neurons (light blue and light red) in region 1, 2, 3 in the image reconstruction task. The threshold for significance is $p \leq 0.05$. The results show that our models (CAE-FRs) provide more significant neurons (red) than the baseline models (blue).

4.2 BIOLOGICAL NEURAL RESPONSES IN CAE-FR IMPROVES IMAGE RECONSTRUCTION

Ten examples of reconstructed images by CAE-FR with neural responses in brain region 3 are presented in Fig. 2. It is obvious that CAE-FR models, no matter which layer the neural response is mapped to, can better reconstruct the original images compared with the standard CAE. The results of the brain region 1 and 2 are illustrated in Appendix Fig. 6 and Fig. 7. The quantitative comparisons of image reconstruction performance are listed in Table 2. It shows that CAE-FR$_1$, CAE-FR$_4$, and CAE-FR$_2$ achieve the best performance when the network gets information from the neurons in the regions 1, 2, and 3, respectively.

Fig. 2 and Table 2 suggests that the information from biological neurons could help CAE-FR for image reconstruction. Further questions are *under what circumstances* and *to what extent* CAE-FR

---

[1]The up arrow ↑ indicates that the higher the value, the better, and the down arrow ↓ indicates that the lower, the better.

Table 4: Pearson correlation between the representations of artificial and biological neurons in region 1, 2, and 3, respectively. The best result in each region under different layers of the model is highlighted with boldface.

Model / Region	CNN-FR$_1$	CAE-FR$_1$	CNN-FR$_2$	CAE-FR$_2$	CNN-FR$_3$	CAE-FR$_3$	CNN-FR$_4$	CAE-FR$_4$
Region 1	0.341	**0.346**	0.467	**0.476**	0.454	**0.455**	0.441	**0.463**
Region 2	0.257	**0.281**	0.384	**0.400**	0.333	**0.338**	0.301	**0.345**
Region 3	0.246	**0.260**	0.361	**0.388**	0.372	**0.404**	0.385	**0.393**

is beneficial from the neural response. Our hypothesis is that *only the biological neurons with high representation similarity to artificial neurons can provide information and contribute to CAE-FR.*

To test our hypothesis, we identify the biological neurons that significantly correlate with the artificial neurons in the CAE-FR model, as well as the insignificant neurons in each brain region. Fig. 4 shows the number of significant neurons and insignificant neurons in region 3 in the IR task. The numbers for region 1&2 are in Appendix Fig. 8. Then, we train the CAE-FRs with the information from these two groups of neurons in region 3 for the IR task separately. The quantitative results of the three metrics are shown in Table 3, confirming that the significant neurons largely improve the IR performance. In contrast, the insignificant neurons jeopardize CAE-FR, resulting in even worse IR performance (see results of Regions 3 in Table 2). These experiments verify our hypothesis, indicating that information from significant neurons can better guide CAE-FR to reconstruct images.
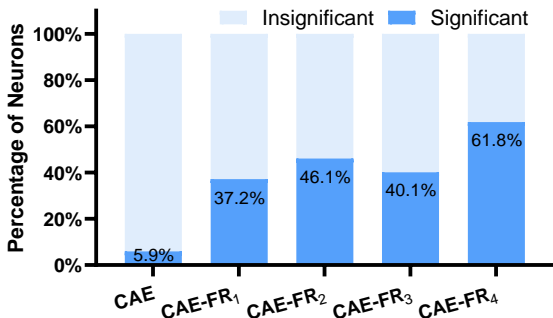

Figure 4: The number of significant neurons and insignificant neurons of the Region 3 in the image reconstruction task. The threshold for significance is $p \leq 0.05$.

4.3 IMAGE RECONSTRUCTION IN CAE-FR IMPROVES NEURAL REPRESENTATION SIMILARITY

Here, we test image reconstruction's effects on neural representation similarity in CAE-FR. The results of the Pearson correlation coefficient between the neural representation of artificial neurons and of biological neurons in region 1, region 2 and region 3 are shown in Table 4. Our models (*i.e.*, CAE-FR$_i$) obtain larger PCC in all three regions compared to the baseline models without the image reconstruction loss (*i.e.*, CNN-FR$_i$). The results show that image reconstruction in our model favors neural representation similarity. This phenomenon seems counter-intuitive as there is a tradeoff between the IR loss and the NSR loss in Eq. equation 3. We hypothesize that *the benefit may stem from feature learning for image reconstruction by CAE: more biological neurons would share representation similarity with artificial neurons when adding image reconstruction loss.* In fact, our experimental results verify the hypothesis (Fig. 3), suggesting that image reconstruction loss can help CAE-FR to improve neural representation similarity between artificial neurons and biological neurons.

4.4 GENERALIZABILITY ACROSS VARIANTS OF CNM AND DAE

To investigate the generalizability of DAE-NR variants, we compare different DAE-NR variants with baseline CNMs and DAEs on IR and NRS tasks, respectively.

Comparisons in IR task: Table 5 provides the quantitative comparisons among different models. Specifically, we compare different CNMs variants (*i.e.*, CAE-FR$_i$, CAE-FC$_i$, and CAE-FM$_i$) with the standard CAE on the IR task. The results show that the best performance is achieved when the network leverages information from biological neurons in Region 3. Moreover, to examine generalizability in other DAE variants, we implement some VAE variants (VAE-FR$_i$, VAE-FC$_i$, and

VAE-FM$_i$) and VQ-VAE variants (VQ-VAE-FR$_i$, VQ-VAE-FC$_i$, and VQ-VAE-FM$_i$) and compare their performance with the standard VAE and VQ-VAE on the IR task, respectively. Our results show that DAE-NR, VAE variants, and VQ-VAE variants that use information from biological neurons have better IR performances than baseline models.

Comparisons in NSR task: Pearson correlation coefficient (PCC↑) between the neural representation of artificial and biological neurons in region 1, region 2, and region 3 are shown in Table 6. To verify the effect of different DAEs for CNN-FR, we compare the variants of CAE (CAE-FR$_i$, CAE-FC$_i$, and CAE-FM$_i$) with CNN-FR on the NSR task. Our models obtain higher PCC in all three regions compared to the baseline models. Furthermore, to validate the function of other CNM variants with different constraints of DAEs, we apply the variants of CNN-FC (CAE-FC$_i$, VAE-FC$_i$, and VQ-VAE-FC$_i$) and the variants of CNN-FM (CAE-FM$_i$, VAE-FM$_i$, and VQ-VAE-FM$_i$) to compare the performance on the NRS task, respectively. Our results show that the biologically-inspired variants of both CNN-FC and CNN-FM via our DAE-NR framework have a better performance than the original models.

Table 5: Quantitative results of image reconstruction with all neurons in the region 3. The best results under different metrics for each region are highlighted in bold.

$\mathbf{h}_i$	$\mathbf{h}_1$			$\mathbf{h}_2$			$\mathbf{h}_3$			$\mathbf{h}_4$		
Metric / Model	MSE↓	PSNR↑	SSIM↑	MSE↓	PSNR↑	SSIM↑	MSE↓	PSNR↑	SSIM↑	MSE↓	PSNR↑	SSIM↑
CAE$_i$	0.074	17.289	0.593	0.074	17.289	0.593	0.074	17.289	0.593	0.074	17.289	0.593
CAE-FR$_i$ (**Ours**)	**0.043**	19.832	0.764	**0.043**	**19.852**	**0.767**	0.045	19.698	0.758	0.051	19.107	0.718
CAE-FC$_i$ (**Ours**)	**0.043**	**19.876**	**0.768**	0.044	19.811	0.763	0.061	18.290	0.734	**0.044**	**19.802**	**0.760**
CAE-FM$_i$ (**Ours**)	0.045	19.692	0.761	**0.043**	19.843	0.764	**0.044**	**19.818**	**0.761**	**0.044**	19.757	0.757
VAE$_i$	0.104	15.983	0.402	0.104	15.983	0.402	0.104	15.983	0.402	0.104	15.983	0.402
VAE-FR$_i$ (**Ours**)	**0.101**	**16.106**	0.414	**0.101**	16.066	0.409	**0.101**	16.083	**0.417**	0.102	16.063	0.414
VAE-FC$_i$ (**Ours**)	0.103	16.003	0.412	**0.101**	16.094	0.412	**0.101**	**16.096**	0.416	**0.101**	**16.089**	**0.418**
VAE-FM$_i$ (**Ours**)	0.102	16.046	**0.415**	**0.101**	16.073	**0.414**	0.102	16.025	0.413	0.103	16.017	0.412
VQ-VAE$_i$	0.082	16.959	0.497	0.082	16.959	0.497	0.082	16.959	0.497	0.082	16.959	0.497
VQ-VAE-FR$_i$ (**Ours**)	0.071	17.636	0.569	0.069	17.741	0.568	0.073	17.487	**0.557**	0.071	17.581	0.560
VQ-VAE-FC$_i$ (**Ours**)	0.076	17.264	0.526	0.075	17.324	0.525	**0.072**	**17.539**	0.547	**0.067**	**17.839**	**0.581**
VQ-VAE-FM$_i$ (**Ours**)	0.068	**17.782**	**0.572**	**0.068**	**17.791**	**0.571**	0.091	16.496	0.546	0.072	17.508	0.542

Table 6: Results of PCC↑ between the representations of artificial and biological neurons in three brain regions. The best results are highlighted in bold.

Region	Region 1				Region 2				Region 3			
$\mathbf{h}_i$ / Model	$\mathbf{h}_1$	$\mathbf{h}_2$	$\mathbf{h}_3$	$\mathbf{h}_4$	$\mathbf{h}_1$	$\mathbf{h}_2$	$\mathbf{h}_3$	$\mathbf{h}_4$	$\mathbf{h}_1$	$\mathbf{h}_2$	$\mathbf{h}_3$	$\mathbf{h}_4$
CNN-FR$_i$	0.335	0.455	0.432	0.431	0.254	0.375	0.309	0.305	0.244	0.348	0.350	0.359
CAE-FR$_i$ (**Ours**)	0.338	0.471	0.449	**0.452**	0.277	**0.396**	0.319	0.348	0.254	0.377	**0.397**	0.394
VAE-FR$_i$ (**Ours**)	0.338	**0.479**	0.455	0.450	0.277	0.386	0.317	0.342	**0.269**	0.375	0.382	**0.404**
VQ-VAE-FR$_i$ (**Ours**)	**0.349**	0.470	**0.463**	0.444	**0.295**	0.388	**0.337**	**0.349**	0.261	**0.394**	0.382	0.387
CNN-FC$_i$	0.343	0.349	0.397	0.435	0.247	0.268	0.292	0.328	0.325	0.316	0.344	0.374
CAE-FC$_i$ (**Ours**)	**0.349**	0.382	0.415	**0.438**	**0.266**	0.281	0.319	0.341	0.335	**0.341**	0.384	0.399
VAE-FC$_i$ (**Ours**)	0.340	**0.383**	**0.418**	**0.438**	0.255	**0.290**	**0.321**	0.343	0.337	0.337	0.379	0.398
VQ-VAE-FC$_i$ (**Ours**)	0.347	0.377	0.415	0.434	0.264	0.289	0.313	**0.361**	**0.338**	**0.341**	**0.388**	**0.427**
CNN-FM$_i$	0.150	0.222	0.110	0.220	0.123	0.186	0.127	0.162	0.064	0.140	0.102	0.178
CAE-FM$_i$ (**Ours**)	**0.154**	0.235	0.115	0.227	0.134	0.222	**0.144**	**0.182**	0.073	0.171	0.109	**0.203**
VAE-FM$_i$ (**Ours**)	0.149	0.238	**0.125**	**0.240**	**0.136**	**0.224**	0.131	0.176	**0.074**	**0.172**	**0.111**	0.201
VQ-VAE-FM$_i$ (**Ours**)	0.153	**0.239**	0.115	0.221	0.135	0.221	0.136	0.162	0.069	0.162	**0.111**	0.200

Together, we demonstrate that the DAE-NR has a good generalization in variants of CNM and DAE. Adding neural information to guide DAE can help reconstruct visual stimuli; in turn, integrating image reconstruction loss into CNM can improve the representation similarity between artificial and biological neurons.

5 CONCLUSION

In this study, we proposed the DAE-NRs, a hybrid framework that integrates the neural response into deep autoencoder models. Inspired by CNN-based neural activity prediction models in computational neuroscience Klindt et al. (2017); Bashivan et al. (2019), we leveraged a Poisson loss to bring neural information to a specific layer of DAE, resulting in better image reconstruction performance. In turn, the IR task facilitates feature learning in DAE and leads to higher neural representation

similarity between biological and artificial neurons. Our work bridges the gap between DAE for image reconstruction and CNM for neural representation similarity.

Broader impact Besides the image reconstruction task and neural representation similarity task, DAE-NR could enable many other potential applications in the future. For instance, DAE-NR provides a more natural way to synthesize images that maximize or control neural activity, compared with the method proposed by Bashivan et al. (2019). Also, DAE-NR can serve as a data engine for biological experiments, synthesizing neural responses to visual stimuli. Moreover, it is important to investigate the generalizability of DAE-NR on variants of auto-encoder Larsen et al. (2016); Khattar et al. (2019); Park et al. (2020); Wang et al. (2021); Cai et al. (2021), on various types of stimuli (*e.g.*, sound and face) and in other tasks (*e.g.*, classification, generation and detection Ran et al. (2021)). Although we only tested DAE-NR with mice neural data, the DAE-NR framework can be easily extended to the neurons in primates (*e.g.*, monkey Zhang et al. (2021) or humans). DAE-NR opens a new window for combining artificial intelligence and brain intelligence.

REFERENCES

Ján Antolík, S. Hofer, J. Bednar, and T. Mrsic-Flogel. Model constrained by visual hierarchy improves prediction of neural responses to natural scenes. *PLoS Computational Biology*, 12, 2016.

P. Bashivan, Kohitij Kar, and J. DiCarlo. Neural population control via deep image synthesis. *Science*, 364, 2019.

Santiago A. Cadena, George H Denfield, Edgar Y. Walker, Leon A. Gatys, A. Tolias, M. Bethge, and Alexander S. Ecker. Deep convolutional models improve predictions of macaque v1 responses to natural images. *PLoS Computational Biology*, 15, 2019.

Yujun Cai, Yiwei Wang, Yiheng Zhu, Tat-Jen Cham, Jianfei Cai, Junsong Yuan, Jun Liu, Chuanxia Zheng, Sijie Yan, Henghui Ding, et al. A unified 3d human motion synthesis model via conditional variational auto-encoder. In *Proceedings of the IEEE/CVF International Conference on Computer Vision*, pp. 11645–11655, 2021.

Matteo Carandini, Jonathan B Demb, Valerio Mante, David J. Tolhurst, Yang Dan, Bruno A. Olshausen, Jack L. Gallant, and Nicole C. Rust. Do we know what the early visual system does? *The Journal of Neuroscience*, 25:10577 – 10597, 2005.

Gautham P Das, Philip J Vance, Dermot Kerr, Sonya A Coleman, Thomas M McGinnity, and Jian K Liu. Computational modelling of salamander retinal ganglion cells using machine learning approaches. *Neurocomputing*, 325:101–112, 2019.

J. DiCarlo, D. Zoccolan, and N. Rust. How does the brain solve visual object recognition? *Neuron*, 73:415–434, 2012.

Ursula C. Dräger. Receptive fields of single cells and topography in mouse visual cortex. *Journal of Comparative Neurology*, 160, 1975.

Callie Federer, Haoyan Xu, Alona Fyshe, and Joel Zylberberg. Improved object recognition using neural networks trained to mimic the brain's statistical properties. *Neural networks : the official journal of the International Neural Network Society*, 131:103–114, 2020.

Emmanouil Froudarakis, Philipp Berens, Alexander S. Ecker, R. James Cotton, Fabian H Sinz, Dimitri Yatsenko, Peter Saggau, Matthias Bethge, and Andreas Savas Tolias. Population code in mouse v1 facilitates read-out of natural scenes through increased sparseness. *Nature neuroscience*, 17:851 – 857, 2014.

K. Fukushima, S. Miyake, and T. Ito. Neocognitron: A neural network model for a mechanism of visual pattern recognition. *IEEE Transactions on Systems, Man, and Cybernetics*, SMC-13:826–834, 1983.

Ian Goodfellow, Yoshua Bengio, and Aaron Courville. *Deep learning*. MIT press, 2016.

Geoffrey E Hinton and Ruslan R Salakhutdinov. Reducing the dimensionality of data with neural networks. *science*, 313(5786):504–507, 2006.

David H Hubel and Torsten N Wiesel. Receptive fields, binocular interaction and functional architecture in the cat's visual cortex. *The Journal of physiology*, 160(1):106–154, 1962.

David H. Hubel and Torsten N. Wiesel. Receptive fields and functional architecture of monkey striate cortex. *The Journal of Physiology*, 195, 1968.

Dhruv Khattar, Jaipal Singh Goud, Manish Gupta, and Vasudeva Varma. Mvae: Multimodal variational autoencoder for fake news detection. In *The world wide web conference*, pp. 2915–2921, 2019.

Diederik P. Kingma and Max Welling. Auto-encoding variational bayes. *International Conference on Learning Representations(ICLR)*, 2014.

David A Klindt, Alexander S Ecker, Thomas Euler, and Matthias Bethge. Neural system identification for large populations separating what and where. In *Advances in Neural Information Processing Systems (NeurIPS)*, pp. 3509–3519, 2017.

A. Krizhevsky, Ilya Sutskever, and Geoffrey E. Hinton. Imagenet classification with deep convolutional neural networks. *Communications of the ACM*, 60:84 – 90, 2012.

Anders Boesen Lindbo Larsen, Søren Kaae Sønderby, Hugo Larochelle, and Ole Winther. Autoencoding beyond pixels using a learned similarity metric. In *International conference on machine learning*, pp. 1558–1566. PMLR, 2016.

Y. LeCun, B. Boser, J. Denker, D. Henderson, R. Howard, W. Hubbard, and L. Jackel. Handwritten digit recognition with a back-propagation network. In *Advances in Neural Information Processing Systems (NeurIPS)*, 1989.

Tom Macpherson, Anne Churchland, Terry Sejnowski, James DiCarlo, Yukiyasu Kamitani, Hidehiko Takahashi, and Takatoshi Hikida. Natural and artificial intelligence: A brief introduction to the interplay between ai and neuroscience research. *Neural Networks*, 2021.

Jonathan Masci, Ueli Meier, Dan Cireşan, and Jürgen Schmidhuber. Stacked convolutional auto-encoders for hierarchical feature extraction. In *International conference on artificial neural networks*, pp. 52–59. Springer, 2011.

Lane McIntosh, Niru Maheswaranathan, Aran Nayebi, Surya Ganguli, and Stephen Baccus. Deep learning models of the retinal response to natural scenes. *Advances in neural information processing systems(NeurIPS)*, 29:1369–1377, 2016.

Arne F Meyer, Ross S Williamson, Jennifer F Linden, and Maneesh Sahani. Models of neuronal stimulus-response functions: elaboration, estimation, and evaluation. *Frontiers in systems neuroscience*, 10:109, 2017.

Cristopher M. Niell, Michael P. Stryker, and Wendell M. Keck. Highly selective receptive fields in mouse visual cortex. *The Journal of Neuroscience*, 28:7520 – 7536, 2008.

Taesung Park, Jun-Yan Zhu, Oliver Wang, Jingwan Lu, Eli Shechtman, Alexei Efros, and Richard Zhang. Swapping autoencoder for deep image manipulation. *Advances in Neural Information Processing Systems*, 33:7198–7211, 2020.

Xuming Ran, Mingkun Xu, Lingrui Mei, Qi Xu, and Quanying Liu. Detecting out-of-distribution samples via variational auto-encoder with reliable uncertainty estimation. *Neural Networks*, 2021.

Saiprasad Ravishankar, J. C. Ye, and Jeffrey A. Fessler. Image reconstruction: From sparsity to data-adaptive methods and machine learning. *Proceedings of the IEEE*, 108:86–109, 2020.

Ryan J. Rowekamp and T. Sharpee. Cross-orientation suppression in visual area v2. *Nature Communications*, 8, 2017.

Shahd Safarani, Arne Nix, Konstantin Friedrich Willeke, Santiago A Cadena, Kelli Restivo, George Denfield, Andreas S Tolias, and Fabian H Sinz. Towards robust vision by multi-task learning on monkey visual cortex. In *Advances in neural information processing systems (NeurIPS)*, 2021.

Martin Schrimpf, Jonas Kubilius, Ha Hong, Najib J. Majaj, Rishi Rajalingham, Elias B. Issa, Kohitij Kar, Pouya Bashivan, Jonathan Prescott-Roy, Kailyn Schmidt, Daniel Yamins, and James J. DiCarlo. Brain-score: Which artificial neural network for object recognition is most brain-like? *bioRxiv*, 2018.

Aäron van den Oord, Oriol Vinyals, and K. Kavukcuoglu. Neural discrete representation learning. In *Advances in Neural Information Processing Systems (NeurIPS)*, 2017.

Pascal Vincent, Hugo Larochelle, Yoshua Bengio, and Pierre-Antoine Manzagol. Extracting and composing robust features with denoising autoencoders. In *Proceedings of the 25th international conference on Machine learning*, pp. 1096–1103, 2008.

William E. Vinje and Jack L. Gallant. Sparse coding and decorrelation in primary visual cortex during natural vision. *Science*, 287 5456:1273–6, 2000.

Brett Vintch, J. Movshon, and Eero P. Simoncelli. A convolutional subunit model for neuronal responses in macaque v1. *The Journal of Neuroscience*, 35:14829 – 14841, 2015.

Edgar Y Walker, Fabian H Sinz, Erick Cobos, Taliah Muhammad, Emmanouil Froudarakis, Paul G Fahey, Alexander S Ecker, Jacob Reimer, Xaq Pitkow, and Andreas S Tolias. Inception loops discover what excites neurons most using deep predictive models. *Nature neuroscience*, 22(12):2060–2065, 2019.

Ge Wang, Jong Chu Ye, Klaus Mueller, and Jeffrey A Fessler. Image reconstruction is a new frontier of machine learning. *IEEE transactions on medical imaging*, 37(6):1289–1296, 2018.

Guojun Wang, Weijun Li, Liping Zhang, Linjun Sun, Peng Chen, Lina Yu, and Xin Ning. Encoder-x: Solving unknown coefficients automatically in polynomial fitting by using an autoencoder. *IEEE Transactions on Neural Networks and Learning Systems*, 2021.

Zhou Wang, Alan Conrad Bovik, Hamid R. Sheikh, and Eero P. Simoncelli. Image quality assessment: from error visibility to structural similarity. *IEEE Transactions on Image Processing*, 13:600–612, 2004.

Michael Weliky, József Fiser, Ruskin H Hunt, and David N Wagner. Coding of natural scenes in primary visual cortex. *Neuron*, 37:703–718, 2003.

B. Willmore, R. Prenger, M. C. Wu, and J. Gallant. The berkeley wavelet transform: A biologically inspired orthogonal wavelet transform. *Neural Computation*, 20:1537–1564, 2008.

Daniel Yamins and J. DiCarlo. Using goal-driven deep learning models to understand sensory cortex. *Nature Neuroscience*, 19:356–365, 2016.

Takashi Yoshida and Kenichi Ohki. Natural images are reliably represented by sparse and variable populations of neurons in visual cortex. *Nature Communications*, 11, 2020.

Jie Zhang, Xiaocang Zhu, Shanshan Wang, Hossein Esteky, Yonghong Tian, Robert Desimone, and Huihui Zhou. Visual attention in the fovea and the periphery during visual search. *bioRxiv*, 2021.

Chengxu Zhuang, Yulong Wang, Daniel Yamins, and Xiaolin Hu. Deep learning predicts correlation between a functional signature of higher visual areas and sparse firing of neurons. *Frontiers in Computational Neuroscience*, 11, 2017.

Chengxu Zhuang, Siming Yan, Aran Nayebi, Martin Schrimpf, Michael C. Frank, J. DiCarlo, and D. Yamins. Unsupervised neural network models of the ventral visual stream. *Proceedings of the National Academy of Sciences of the United States of America*, 118, 2021.

A EXPERIMENTAL SETTINGS

In this section, we introduce the details of the settings in our experiments. Firstly, Table 7 is the number of neural datasets from three brain regions and Fig. 5 illustrates the training image of the neural stimuli. Secondly, the Table 8 and Table 9 are the settings of the hyperparameters for image reconstruction and neural similarity experiments, respectively. Thirdly, the Table 10 is the setting of the hyperparameters of different DAE-NR variants for image reconstruction experiments for image reconstruction on region 3 . Fourthly, the Table 11, Table 12 and Table 13 are the settings the hyperparameters of different DAE-NR variants for neural similarity experiments on Region 1,2 and 3, respectively.

Table 7: The neural dataset containing neural responses in three brain regions under visual stimulation Antolík et al. (2016). The number in bracket is the repeated times.

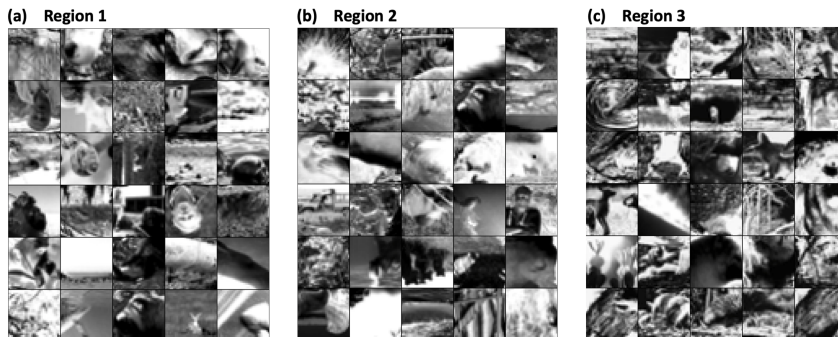|	Number of train images	Number of test images	Number of neurons
Region 1	1800 (1)	50 (10)	103
Region 2	1260 (1)	50 (8)	55
Region 3	1800 (1)	50 (12)	102

Figure 5: The examples of training stimuli in each brain region.

Table 8: The settings of the hyperparameters for image reconstruction experiments.

	Region 1	Region 2	Region 3
Models	$\alpha : \beta$	$\alpha : \beta$	$\alpha : \beta$
CAE-FR$_1$	1e-0:1e-5	1e-0:1e-3	1e-0:1e-4
CAE-FR$_2$	1e-0:1e-5	1e-0:1e-4	1e-0:1e-3
CAE-FR$_3$	1e-0:1e-4	1e-0:1e-3	1e-0:1e-5
CAE-FR$_4$	1e-0:1e-5	1e-0:1e-4	1e-0:1e-4

B ADDITIONAL EXPERIMENTS

In this section, we provide results from additional experiments. Fig. 6 and Fig. 7 display the results of image reconstruction using the neural responses on the region 1 and 2. Fig. 8 shows the number of significant neurons and insignificant neurons of regions 1 and 2 in the image reconstruction experiments, respectively.

Table 9: The settings the hyperparameters for neural similarity experiments.

Models	Region 1 $\alpha : \beta$	Region 2 $\alpha : \beta$	Region 3 $\alpha : \beta$
CAE-FR$_1$	1e-0:9e-1	7e-1:1e-0	8e-1:1e-0
CAE-FR$_2$	7e-1:1e-0	1e-0:1e-2	4e-1:1e-0
CAE-FR$_3$	1e-0:6e-1	1e-4:1e-0	1e-0:4e-1
CAE-FR$_4$	1e-0:9e-1	1e-0:1e-2	1e-0:9e-1

Table 10: The settings the hyperparameters of different DAE-NR variants for image reconstruction experiments on region 3.

Models	h_1 $\alpha : \beta$	h_2 $\alpha : \beta$	h_3 $\alpha : \beta$	h_4 $\alpha : \beta$
CAE-FR	1e-0:1e-4	1e-0:5e-3	1e-0:1e-3	1e-0:1e-3
CAE-FC	1e-0:1e-4	1e-0:1e-4	1e-0:1e-4	1e-0:1e-4
CAE-FM	1e-0:2e-1	1e-0:1e-3	1e-0:1e-4	1e-0:1e-4
VAE-FR	1e-0:2e-2	1e-0:1e-2	1e-0:2e-1	1e-0:5e-3
VAE-FC	1e-0:1e-2	1e-0:5e-3	1e-0:1e-3	1e-0:1e-1
VAE-FM	1e-0:5e-3	1e-0:5e-2	1e-0:2e-1	1e-0:5e-3
VQ-VAE-FR	1e-0:2e-2	1e-0:2e-1	1e-0:1e-2	1e-0:1e-3
VQ-VAE-FC	1e-0:1e-3	1e-0:1e-4	1e-0:1e-4	1e-0:1e-4
VQ-VAE-FM	1e-0:2e-1	1e-0:1e-3	1e-0:1e-2	1e-0:1e-3

Table 11: The settings the hyperparameters of different DAE-NR variants for neural similarity experiments on Region 1

Models	h_1 $\alpha : \beta$	h_2 $\alpha : \beta$	h_3 $\alpha : \beta$	h_4 $\alpha : \beta$
CAE-FR	1e-0:5e-1	1e-0:5e-2	1e-0:5e-2	1e-0:1e-2
VAE-FR	1e-3:1e-0	2e-2:1e-0	1e-3:1e-0	1e-1:1e-0
VQ-VAE-FR	1e-0:2e-2	1e-0:2e-1	1e-0:5e-3	1e-0:2e-1
CAE-FC	5e-3:1e-0	1e-3:1e-0	2e-2:1e-0	1e-2:1e-0
VAE-FC	2e-2:1e-0	1e-0:1e-2	2e-1:1e-0	1e-3:1e-0
VQ-VAE-FC	1e-0:1e-1	1e-0:5e-1	1e-4:1e-0	1e-2:1e-0
CAE-FM	1e-2:1e-0	5e-1:1e-0	1e-0:1e-1	1e-0:5e-1
VAE-FM	1e-4:1e-0	1e-3:1e-0	1e-1:1e-0	1e-1:1e-0
VQ-VAE-FM	1e-1:1e-0	1e-1:1e-0	1e-0:1e-2	1e-0:1e-0

Table 12: The settings the hyperparameters of different DAE-NR variants for neural similarity experiments on Region 2

Models	h_1 $\alpha : \beta$	h_2 $\alpha : \beta$	h_3 $\alpha : \beta$	h_4 $\alpha : \beta$
CAE-FR	1e-0:2e-1	1e-0:2e-2	5e-3:1e-0	1e-0:5e-3
VAE-FR	5e-3:1e-0	2e-1:1e-0	5e-2:1e-0	5e-1:1e-0
VQ-VAE-FR	1e-0:1e-1	2e-1:1e-0	1e-0:1e-2	1e-0:2e-1
CAE-FC	1e-2:1e-0	5e-3:1e-0	1e-0:5e-2	1e-4:1e-0
VAE-FC	1e-2:1e-0	5e-3:1e-0	1e-0:5e-1	1e-4:1e-0
VQ-VAE-FC	1e-0:1e-0	5e-3:1e-0	1e-3:1e-0	1e-3:1e-0
CAE-FM	1e-0:1e-1	1e-0:1e-2	1e-0:5e-3	1e-0:5e-3
VAE-FM	5e-2:1e-0	1e-4:1e-0	5e-3:1e-0	2e-2:1e-0
VQ-VAE-FM	1e-0:5e-2	5e-2:1e-0	1e-0:1e-1	1e-0:5e-1

Table 13: The settings the hyperparameters of different DAE-NR variants for neural similarity experiments on Region 3

	h_1	h_2	h_3	h_4
Models	$\alpha : \beta$	$\alpha : \beta$	$\alpha : \beta$	$\alpha : \beta$
CAE-FR	1e-0:1e-1	1e-0:1e-0	1e-0:5e-2	1e-0:1e-2
VAE-FR	1e-0:1e-4	5e-1:1e-0	1e-2:1e-0	1e-0:1e-0
VQ-VAE-FR	1e-0:2e-1	1e-0:2e-2	1e-0:1e-0	1e-4:1e-0
CAE-FC	1e-0:2e-1	5e-2:1e-0	1e-0:1e-1	1e-0:2e-1
VAE-FC	1e-3:1e-0	1e-2:1e-0	5e-3:1e-0	2e-1:1e-0
VQ-VAE-FC	1e-1:1e-0	1e-3:1e-0	1e-2:1e-0	1e-4:1e-0
CAE-FM	5e-3:1e-0	1e-0:5e-3	1e-0:5e-1	1e-2:1e-0
VAE-FM	1e-3:1e-0	1e-0:2e-1	2e-2:1e-0	5e-2:1e-0
VQ-VAE-FM$_4$	1e-0:5e-1	1e-4:1e-0	1e-3:1e-0	1e-3:1e-0
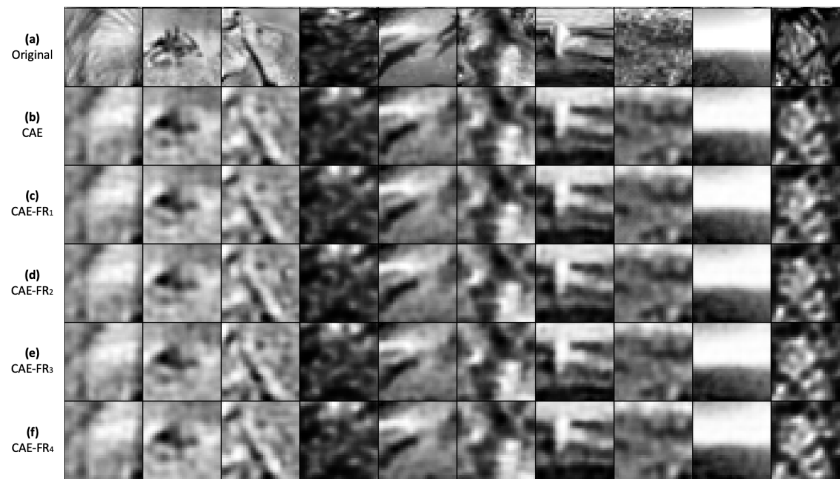
Figure 6: The reconstructed images with neurons in Region 1. From top to bottom, each row displays the original images (a), the images reconstructed by CAE (b), CAE-FR$_1$ (c), CAE-F$_2$ (d), CAE-F$_3$ (e), CAE-FR$_4$ (f), respectively.
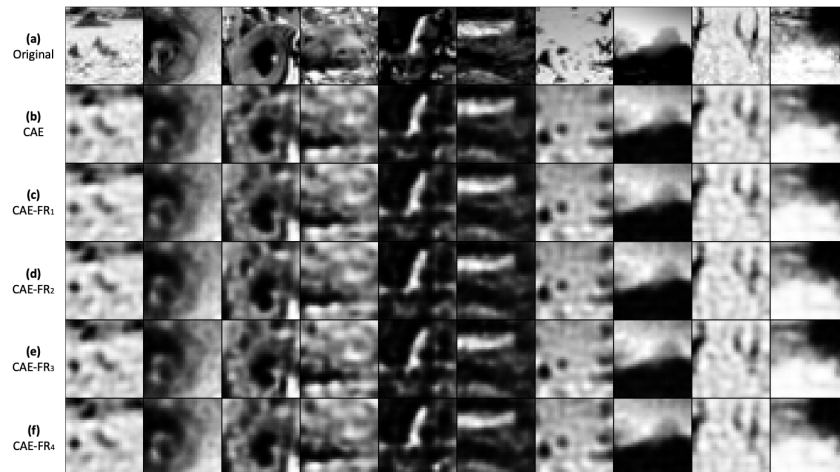
Figure 7: The reconstructed images with neurons in Region 2. From top to bottom, each row displays the original images (a), the images reconstructed by CAE (b), CAE-FR$_1$ (c), CAE-F$_2$ (d), CAE-F$_3$ (e), CAE-FR$_4$ (f), respectively.
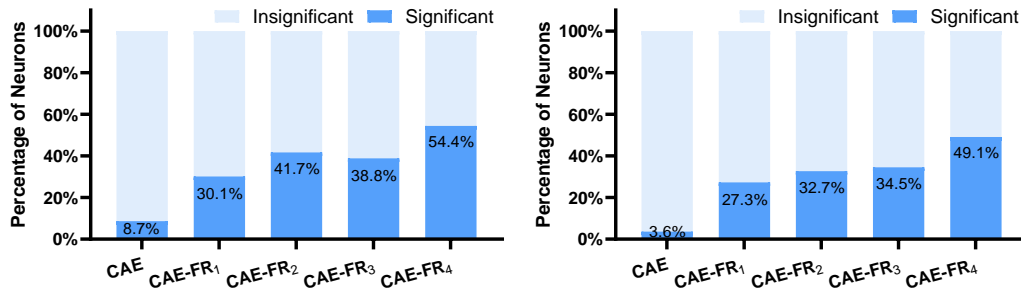
Figure 8: The number of significant neurons and insignificant neurons in region 1 and 2 in the image reconstruction experiments. The threshold for significance is $p \leq 0.05$.